PAPER

Check for updates

In situ synthesis of nitrogen-doped carbon dots in the interlayer region of a layered double hydroxide with tunable quantum yield†

Wendi Liu, Simin Xu, Ruizheng Liang,* Min Wei, [iD] * David G. Evans and Xue Duan

Carbon dots (CDs) have drawn considerable research interest due to their fascinating physicochemical properties and optical performance. Herein, we report the preparation of nitrogen-doped carbon dots (N-CDs) *via* an *in situ* hydrothermal reaction of citric acid (CA) and ethylenediamine (EDA) in the confined two-dimensional gallery of a layered double hydroxide (LDH). The resulting N-CDs/LDH material shows a long-range ordered structure, with blue-emissive, sheet-like ultrathin N-CDs ($\sim$0.62 nm) accommodated in the LDH gallery. In particular, the photoluminescence quantum yield (PLQY) can be tuned by adjusting the charge density of the LDH host layer, and the maximum value accomplishes 61.63%. This variable performance is attributed to different N-doping contents, which is confirmed by X-ray photoelectron spectroscopy (XPS), elemental analysis and molecular dynamics (MD) simulations. Moreover, the N-CDs/LDH composite exhibits temperature-responsive emission under sub-zero conditions (from -150 °C to 0 °C). Its potential application is demonstrated by incorporating N-CDs/LDH within a polyvinyl alcohol (PVA) polymer matrix, which is then used as a modulator to transfer ultraviolet light to blue emission. This work provides a facile method for the preparation of highly luminescent N-CD-based solid-state materials through an *in situ* interlayer reaction, which can serve as promising candidates in optical and display devices.

Introduction

CDs, a new kind of zero-dimensional carbon nanomaterial, have received extensive attention due to their excellent optical performance, good aqueous solubility and environmental friendliness.[1,2] It has been recognized that doping carbon dots with heteroatoms, especially the nitrogen atom, markedly improves the fluorescence properties (*e.g.*, enhanced PLQY[3] and modulated absorption/emission position[4]), since a nitrogen atom would produce extra valence states or defects when introduced in the carbon structure.[5] The synthesized N-CDs have been applied in various fields including bioimaging, sensors, photonic or optoelectronic devices.[6,7] However, the previous studies mainly focused on the synthesis of N-CDs *via* various nitrogenous precursors in aqueous solutions, and aggregation induced fluorescence quenching normally occurred under solid-state conditions. Moreover, it is difficult to precisely control the nitrogen doping level so as to promote the fluorescence properties. Therefore, how to acquire N-CD based solid-state materials

with excellent PLQY and tunable fluorescence properties by material design and synthesis exploration remains a big challenge.

LDHs are a class of two-dimensional inorganic materials represented by the general formula $[M_{1-x}^{2+}M_x^{3+}(OH)_2](A^{n-})_{x/n} \cdot mH_2O$, consisting of positively-charged brucite-like layers and exchangeable interlayer anions (M^{2+} and M^{3+} are di- and trivalent metal cations, and A^{n-} is the charge-balancing anion).[8,9] Recently, the interlayer gallery of LDHs as a nanoreactor for confined synthesis of carbon nanorings and Au nanosheets has drawn much interest.[10] Moreover, it is reported that the dispersity and stability of organic species can be highly improved after their intercalation into the LDH interlamellar region.[11] This motivates us to co-intercalate the carbon precursor and the nitrogen source into the LDH gallery, followed by triggering an interlayer reaction so as to obtain a new N-CDs/LDH composite. The resulting material would exhibit the following advantages: (1) the 2D architecture of the LDH provides a confined reaction microenvironment for the *in situ* synthesis of N-CDs, which would facilitate a uniform dispersion and avoid aggregation induced quenching; (2) the nitrogen doping level and PLQY of N-CDs can be precisely controlled through adjusting the charge density of the LDH host layer; (3) the N-CDs/LDH composite may own enhanced stability compared with pristine N-CDs, which would guarantee its practical application.

In this work, a highly-emissive blue N-CDs/LDH composite material was prepared by an *in situ* hydrothermal reaction

State Key Laboratory of Chemical Resource Engineering, Beijing Advanced Innovation Center for Soft Matter Science and Engineering, Beijing University of Chemical Technology, Beijing 100029, China. E-mail: liangruizheng2000@163.com, weimin@mail.buct.edu.cn; Fax: +86-10-64425358; Tel: +86-10-64412131

between EDA and CA intercalated in the LDH interlamellar region. The as-synthesized N-CDs/LDH composite shows a long-range ordered structure, with sheet-like ultrathin N-CDs (~0.62 nm) accommodated in the LDH interlayer region revealed by XRD, TEM and AFM. It is interesting that the PLQY of the N-CDs/LDH composite can be tuned by adjusting the hydrothermal temperature or charge density of the LDH host layer; and the maximum reaches as high as 61.63%, which is among the highest values of CD-based solid-state materials reported so far.[12–14] The enhanced fluorescence performance is attributed to the monodispersed N-CDs with a high level of nitrogen doping confined in the LDH gallery, which is confirmed by electrochemical impedance spectroscopy, elemental analysis and XPS spectra. The N-CDs/LDH composite exhibits temperature-dependent luminescence under sub-zero conditions. Moreover, its potential application is demonstrated through incorporating the N-CDs/LDH within a PVA polymer matrix, which is employed with a commercial ultraviolet light-emitting diode (LED) chip to give strong blue-emitting light.

Results and discussion

Morphological and structural studies on N-CDs/LDH

The N-CDs/LDH composite material is synthesized via a two-step procedure shown in Scheme 1: intercalation of CA into the MgAl-LDH gallery, followed by a further hydrothermal reaction of CA/LDH and EDA to obtain the final product N-CDs/LDH. This method was inspired by the ''bottom up'' approach to aqueous CDs reported by Yang's group, and a polymerization and carbonization process is involved in the hydrothermal reaction of CA and EDA.[3a,15] The XRD pattern of CA/LDH (Fig. 1A) displays a basal reflection at $2\theta = 7.53°$, illustrating a periodic layered structure with a repeated thickness of 1.17 nm. By subtracting the thickness of an LDH host monolayer (0.48 nm), the interlayer gallery of 0.69 nm agrees well with the size of the CA molecule. After the hydrothermal reaction with EDA, the interlayer CA transformed into N-CDs in the confined 2D microenvironment through a polymerization and carbonization process. The XRD pattern of the as-obtained N-CDs/LDH shows no obvious change compared with the precursor CA/LDH. Fourier transform infrared spectroscopy (FT-IR), XPS spectra and solid state ^{13}C NMR are used to verify the occurrence of interlayer reaction. The IR spectrum of N-CDs/LDH
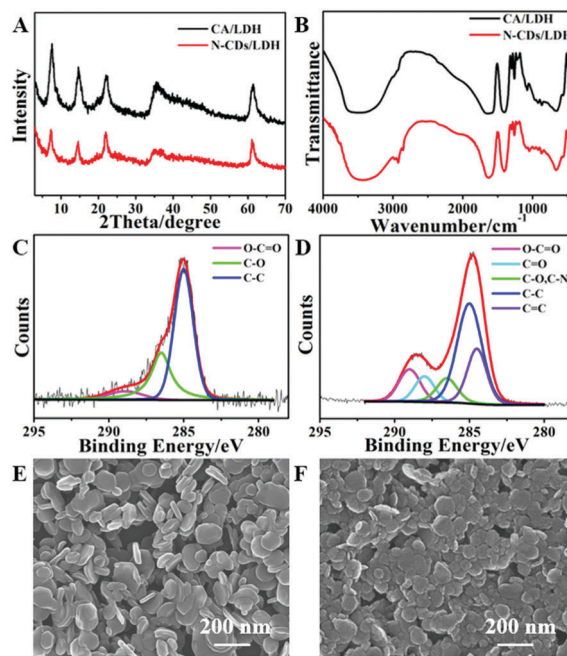
Fig. 1 (A) XRD patterns and (B) FT-IR spectra of CA/LDH and N-CDs/LDH; C1s XPS spectra of (C) CA/LDH and (D) N-CDs/LDH; SEM images of (E) CA/LDH and (F) N-CDs/LDH.

shows an obvious vibration band of the methylene group at 2923 cm^{-1} and 2854 cm^{-1}, suggesting the intercalation and reaction of EDA with CA/LDH (Fig. 1B). XPS spectra of CA/LDH and N-CDs/LDH are shown in Fig. 1C and D respectively. The high resolution C1s spectrum of CA/LDH displays three main peaks: the binding energy at 285.0 eV confirms the sp[3] C–C in the CA molecule; the second peak at 286.5 eV suggests the presence of C–O and the third peak at 288.9 eV is assigned to O–C=O. In the case of N-CDs/LDH, two new binding energy peaks at 288.0 eV and 284.5 eV are observed, suggesting the formation of N-CDs with C=O and C=C groups (Fig. 1D). Moreover, a predominant peak at 399.7 eV ascribed to N1s appears, which is absent in CA/LDH, illustrating the doping of the nitrogen atom in the carbon structure (Fig. S1, ESI†). The solid state ^{13}C NMR spectrum of N-CDs/LDH shows largely decreased signals of original CA, accompanied by a new signal at ~164 ppm attributed to sp[2] carbon species (Fig. S2, ESI†), further confirming the occurrence of interlayer reaction. Fig. 1E displays the scanning electron microscope (SEM) image of CA/LDH, with dispersive and uniform nanoplatelets with a particle size of ~120 nm. After the interlayer hydrothermal reaction, the original morphology is well maintained in the N-CDs/LDH sample (Fig. 1F). Energy dispersive X-ray spectroscopy (EDX) mapping analysis for N-CDs/LDH (Fig. S3, ESI†) shows that Mg, Al, C, O and N are homogeneously distributed. The hydrodynamic particle size of CA/LDH and N-CDs/LDH are 107.7 nm and 105.7 nm (Fig. S4, ESI†), close to the results detected by SEM. Furthermore, the zeta potential of N-CDs/LDH exhibits a slightly positive shift relative to CA/LDH (from −17.5 mV to −14.6 mV, Fig. S5, ESI†), as a result of the interlayer reaction between CA and EDA molecules.
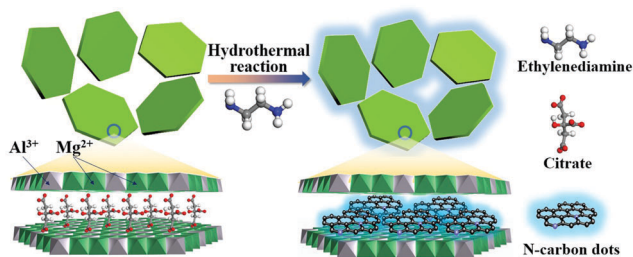
Scheme 1 Schematic representation of the preparation of the N-CDs/LDH composite material.

This journal is © The Royal Society of Chemistry 2017

J. Mater. Chem. C, 2017, 5, 3536–3541 | 3537

In comparison with the non-emissive CA/LDH, the N-CDs/LDH sample gives a bright blue fluorescence at 440 nm, and its photograph exhibits a rather strong brightness under UV light radiation (Fig. S6, ESI†). Thus, it is imperative to investigate the product in the LDH interlamination after hydrothermal reaction. The LDH matrix was etched with hydrochloric acid to obtain the interlayer species. After a dialysis treatment, the solution displays a blue fluorescence at 440 nm with a PLQY of 37.45% (Fig. 2A). The TEM image shows that the produced N-CDs possess an average diameter of ~ 5.8 nm with a high monodispersion (Fig. 2B). The HRTEM image displays a lattice fringe of 0.21 nm in a single particle, which is assigned to the graphite (100) plane (Fig. 2C). The AFM image reveals a thickness of ~ 0.62 nm for a single N-CD sheet (Fig. S7, ESI†). The results demonstrate a plate-like morphology for N-CDs synthesized by interlayer reaction, instead of spherical CDs by a conventional hydrothermal method. Moreover, the FT-IR spectrum indicates the existence of carbonyl and methylene groups and the amide bond, further demonstrating the formation of N-CDs (Fig. S8A, ESI†). The XRD pattern of N-CDs displays a broad peak at 2θ 20–30°, which is attributed to the amorphous graphite lattice (Fig. S8B, ESI†). The Raman spectrum also confirms the graphene structure of N-CDs, with a G band at 1597 cm^{-1} owing to sp^2 bonded carbon and a D band at 1350 cm^{-1} due to the presence of disordered carbon (Fig. 2D) In addition, we compared the ^{1}H-NMR and ^{13}C-NMR spectra of N-CDs prepared by the conventional hydrothermal method and by this 2D interlayer reaction (Fig. S9, ESI†). Obvious differences are found, especially in the high chemical shift region, illustrating that the 2D confined environment imposes an influence on the structural transformation and the carbonization process.

Fluorescence properties of N-CDs/LDH with control over nitrogen doping

As far as we know, reaction temperature is a very important factor for the polymerization and carbonization process leading to N-CDs. We firstly investigate the influence of hydrothermal temperature on the fluorescence properties in the conversion from CA/LDH to N-CDs/LDH through 3D fluorescence spectra. In 3D fluorescence spectra, the horizontal coordinates and vertical coordinates represent the emission wavelength and excitation wavelength respectively; while the intensity is displayed with different colors, which can visually describe the entire fluorescence characteristic of luminescent materials and is extensively used for the overview of multi-component fluorophores. Fig. S10 (ESI†) shows the 3D fluorescence spectra of N-CDs/LDH with different hydrothermal temperatures from 125 °C to 225 °C. In the hydrothermal temperature range 125–150 °C, a constant λ_{ex} at 360 nm and λ_{em} at 440 nm are observed. However, for the N-CDs/LDH composites prepared within the temperature range of 175–200 °C, an excitation-dependent PL emission property is found, possibly due to the formation of multi-luminous centers (Fig. S10C, D and S11, ESI†). In addition, the absolute PLQYs of N-CDs/LDH with different hydrothermal temperatures are measured to be 8.91% (125 °C), 26.16% (150 °C), 21.66% (175 °C), 14.63% (200 °C) and 11.14% (225 °C), respectively (Fig. S10F, ESI†). Taking into account the value of PLQY, the hydrothermal temperature at 150 °C is thus chosen for the following study.

It should be noted that the intercalated density of CA in the MgAl-LDH gallery is determined by the charge density of the host layer (i.e., molar ratio of Mg^{2+}/Al^{3+}); therefore, we studied the fluorescence properties of as-synthesized N-CDs/LDH composites by tuning the Mg^{2+}/Al^{3+} ratio of the LDH matrix within 2–5 (denominated as CA/X-LDH, X = 2–5). After the hydrothermal reaction with the same quantity of EDA at 150 °C, the resulting N-CDs intercalated LDHs are denoted as N-CDs/X-LDH (X = 2–5). Fig. S12A (ESI†) shows the XRD patterns of CA/X-LDH (X = 2–5) materials with a basal spacing of 1.17 nm, indicating the insertion of a CA molecule. After the interlayer hydrothermal reaction, the XRD characteristic reflection shows no obvious change (Fig. S12B, ESI†). All these N-CDs/X-LDH (X = 2–5) samples exhibit bright blue luminescence under UV light (Fig. 3 insets), and the 3D fluorescence spectra show a luminescence center in the blue area with no obvious difference (Fig. 3A–D). The absolute PLQYs of N-CDs/X-LDH (X = 2–5) are measured to be 26.16%, 29.54%, 52.37% and 61.63%, respectively (Fig. 3E). The sample of N-CDs/5-LDH gives the largest PLQY in this work, which is also among the highest performance in solid-state CD-based fluorescent materials compared with previous reports (Table S1, ESI†).

Organic elemental analysis and XPS spectra were used to study the interlayer reaction. As shown in Table S2 (ESI†), the C content in CA/X-LDH (X = 2–5) decreases gradually, indicating that the intercalated density of CA declines along with the decease of charge density of MgAl-LDH (i.e., increase of the Mg^{2+}/Al^{3+} ratio). After the in situ hydrothermal reaction, EDA molecules enter into the interspace of LDHs and react with CA to produce N-doped CDs, which is confirmed by the N content in N-CDs/LDH samples. The N content in N-CDs/X-LDH (X = 2–5) samples increases from 0.48% to 0.76% with the enhancement of the Mg^{2+}/Al^{3+} ratio, and the corresponding N/C ratio increases from 0.043 to 0.12. Moreover, the chemical state

Fig. 2 Characterization of interlayer N-CDs: (A) fluorescence excitation and emission spectra; the inset shows the photographs of N-CD aqueous solution under daylight and UV light irradiation; (B) TEM image with particle size distribution; (C) HRTEM image; (D) Raman spectrum.

3538 | J. Mater. Chem. C, 2017, 5, 3536–3541

This journal is © The Royal Society of Chemistry 2017
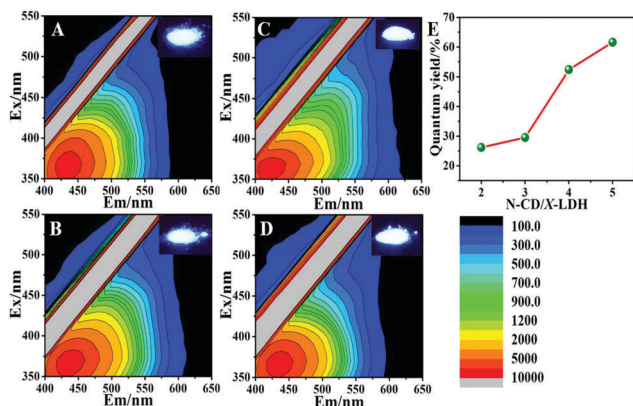
Fig. 3 3D fluorescence spectra (A–D) and PLQYs (E) of N-CDs/X-LDH (X = 2–5) with various Mg^{2+}/Al^{3+} molar ratios. The insets show the corresponding photographs under UV light irradiation.

of the N element in N-CDs/X-LDH (X = 2–5) samples was characterized by the XPS technique. The full XPS spectra of N-CDs/X-LDH (X = 2–5) reveal the signals of Mg, Al, C, O and N elements (Fig. S13, ESI†). In particular, the XPS spectra display a predominant N1s peak at 399.7 eV, which is ascribed to the dopant nitrogen atom in an amide bond (O=C–N) *via* the reaction of –COOH and –NH$_2$ (Fig. 4). This result coincides well with the FT-IR analysis in Fig. S8A (ESI†). Correspondingly, the small binding energy peak at 402.7 eV is due to the unreacted amino N–H bond in the EDA molecule. The relative content of dopant nitrogen (O=C–N) increases from 91.63% to 95.12% based on the integral area calculation, indicating the enhanced nitrogen-doping ability with the increase of the Mg^{2+}/Al^{3+} ratio of LDHs. It is interesting that the PLQY of these N-CDs/LDH composites increase from 26.16% to 61.63% along with the increment of the N doping content. Therefore, LDH serves as an excellent matrix which imposes controlled N-doping, giving rise to a largely enhanced fluorescence emission
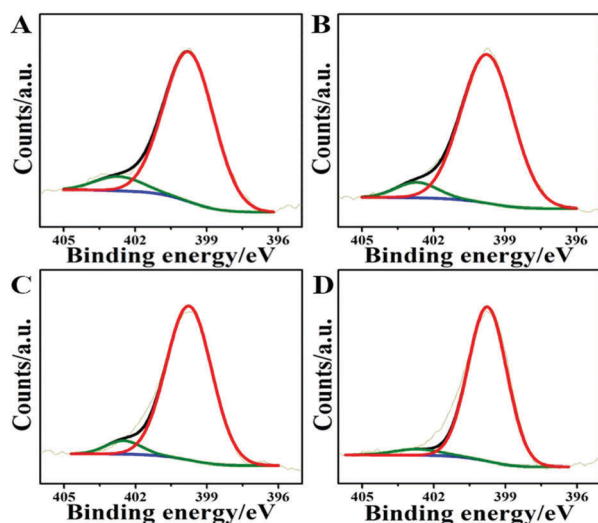
of N-CDs/5-LDH (61.63%). This is even much higher than that of dialyzed N-CDs in water solution (37.45%) from the N-CDs/5-LDH sample, which is possibly due to the inhibited photo-excited charge transfer of N-CDs in the interlayer region of LDHs (Fig. S14, ESI†).

MD simulations to the doping process

MD simulations were performed to investigate the intercalation and diffusion behavior of reactants. The LDH models were constructed according to the chemical composition and charge density of CA/X-LDH (X = 2–5). The chemical compositions were determined by the inductively coupled plasma atomic emission spectroscopy (ICP-AES) and organic elemental analysis (Tables S2 and S3, ESI†). The charge density of the LDH layer can be calculated as $x/(a^2 \cdot \sin 60°)$ where a represents the inherent cation to cation distance within the ab plane and x denotes the molar ratio of $M^{3+}/(M^{3+} + M^{2+})$.[16] Table S4 (ESI†) lists the chemical compositions and charge density of these samples, and the correlation between the N/C molar ratio and charge density is displayed in Fig. S15 (ESI†). Fig. S16 and S17 (ESI†) show the snapshots of CA/X-LDH (X = 2–5) samples after MD simulations, in which the density of the CA molecule decreases along with increasing X. The average dynamic distance between the center carbon atom of adjacent CA molecules is calculated (Fig. 5A–D), which gives 0.675 nm, 0.726 nm, 0.793 nm and 0.829 nm, respectively, in the CA/X-LDH (X = 2–5) models. Therefore, more EDA molecules can enter the LDH gallery with a larger free volume (X = 5), accounting for a higher nitrogen doping of N-CDs/LDH (0.76%). Moreover, the penetration behavior of EDA in the CA/LDH system was further studied by calculating the diffusion coefficient of EDA (Fig. S18, ESI†). According to the recorded dynamics trajectories, the diffusion coefficient of EDA calculated
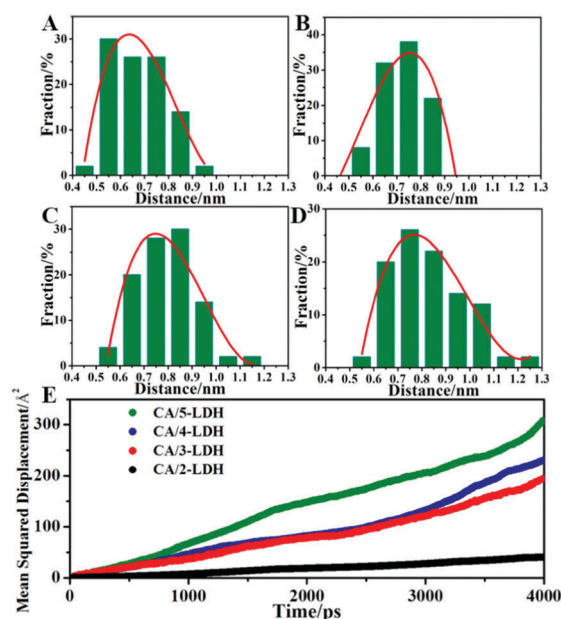
Fig. 5 (A–D) Distance distribution between the central carbon atom of adjacent CA molecules in CA/X-LDH (X = 2–5) models. (E) Mean squared displacement of the EDA molecule in CA/X-LDH (X = 2–5) models over 4000 ps.

Fig. 4 N1s XPS spectra of (A) N-CDs/2-LDH, (B) N-CDs/3-LDH, (C) N-CDs/4-LDH and (D) N-CDs/5-LDH.

with the Einstein equation is 1.72×10^{-7}, 7.34×10^{-7}, 8.74×10^{-7} and 11.88×10^{-7} cm^2 s^{-1} for CA/X-LDH (X = 2–5), respectively (Fig. 5E), indicating an enhanced diffusion ability of EDA in the LDH matrix along with the decrease of layer charge density. By changing the charge density of the LDH host layer, the stoichiometric ratio of interlayer reaction can be tuned, which results in an enhanced N doping and PLQY of N-CDs/LDH.

Potential applications and stability of N-CDs/LDH

Temperature-dependent fluorescence of carbon dots has been discussed by previous researchers.[17] Herein, we studied the *in situ* temperature sensing performance of N-CDs/LDH material by using a microspectrophotometer with a cryostat. At room temperature, the N-CDs/LDH composite material shows an absorption band at 300 nm and a strong blue emission at 440 nm (Fig. 6A). Fig. 6B presents the *in situ* photoluminescence spectra of N-CDs/LDH at various sub-zero temperatures. With the temperature rising from −150 °C to 0 °C, the emission peak intensity of N-CDs/LDH displays an evident decrease and a sensitivity of –0.51% per °C is obtained with a good linear relationship (R^2 = 0.9933). However, the photoluminescence intensity of N-CDs/LDH shows no obvious decline in the range 0–100 °C (Fig. S19, ESI†). This temperature-dependent fluorescent property over −150–0 °C makes N-CDs/LDH composite a promising candidate for low temperature sensing.

In order to further demonstrate the potential application of N-CDs/LDH material in optical displays, an N-CDs/LDH@PVA film was fabricated *via* a solvent evaporation method and its internal structure was studied using a laser scanning confocal microscope. Both the three-dimensional and cross profile graphs show that the film emits uniform and homogeneous blue fluorescence (Fig. 7A, B and Fig. S20, ESI†). Subsequently, this N-CDs/LDH@PVA film was coated on a commercial UV LED chip to obtain a blue light emitting diode (BLED) (shown in Fig. 7C). The UV light from the chip is transformed into blue light when passing through this coating film (Fig. 7D, inset), and the corresponding emission spectrum is shown in Fig. 7D. Fig. 7E illustrates that the Commission Internationale de l'Eclairage (CIE) chromaticity color coordinates of this BLED are (0.1781, 0.1507), which is located in the pure blue region. Moreover, the luminescence intensity of the as-fabricated BLED is rather stable under operation for 12 h (Fig. S21, ESI†).
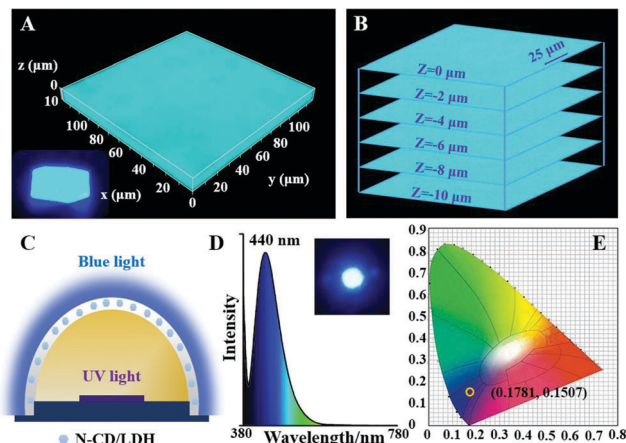
Fig. 7 (A) 3D confocal microscopy image of the N-CDs/LDH@PVA film; the inset shows the photograph of N-CDs/LDH@PVA film under UV light; (B) cross profile microscopy images of the N-CDs/LDH@PVA film with various film thickness; (C) schematic illustration of the N-CDs/LDH@PVA based BLED; (D) emission spectrum and photograph of the BLED under operation conditions (inset); (E) corresponding CIE diagram of the BLED.

UV-resistance capability is a significant parameter for the practical application of luminescent materials. A photostability test was carried out to evaluate the advantages of N-CDs intercalated in the LDH matrix, with an N-CDs@PVA film as a control sample. After *in situ* irradiation with a UV lamp for 3600 s, the real-time fluorescence intensity of the N-CDs/LDH@PVA film shows no obvious decrease; while the N-CDs@PVA film exhibits an 11.6% loss under the same conditions (Fig. S22, ESI†). In addition, bulk N-CDs/LDH@PDMAA (N,N'-dimethylacrylamide) and N-CDs@PDMAA were also prepared *via* introduction of N-CDs/LDH or N-CDs during the polymerization of DMAA, and the superior photostability of N-CDs/LDH is visually demonstrated in the photographs of N-CDs/LDH@PDMAA and N-CDs@PDMAA under high-power UV light irradiation for 2 h (Fig. S23, ESI†). The results confirm that the N-CDs/LDH material owns better photostability than pristine N-CDs, as a result of the suppressed photobleaching of N-CDs within such a 2D confined microenvironment. In addition, the fluorescence intensity of N-CDs/LDH remains stable over 30 days (Fig. S24, ESI†), illustrating an excellent storage stability.

Conclusions

In summary, solid-state N-CD intercalated LDH composites are synthesized through an *in situ* interlayer reaction, which show bright blue luminescence. The resulting N-CDs/LDH composite materials possess a 2D layered structure and ultrathin N-CDs are produced in the LDH gallery during the hydrothermal reaction process. The PLQY of N-CDs/LDH materials can be regulated *via* changing the doping amount of nitrogen in N-CDs revealed by molecular dynamics simulations. The maximal PLQY reaches 61.63%, which is among the highest level of CD-based solid-state materials. Moreover, the N-CDs/LDH composite exhibits temperature-dependent luminescence at low temperatures; the as-prepared N-CDs/LDH@PVA film can be
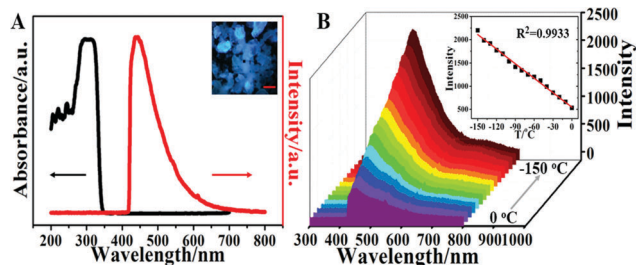
Fig. 6 (A) UV-vis absorption and fluorescence spectrum of N-CDs/LDH detected by a microspectrophotometer; the inset shows the corresponding fluorescence microscopy image with a scale bar of 50 μm. (B) *In situ* fluorescence spectra of N-CDs/LDH in the range from −150 °C to 0 °C; the inset displays the linear correlation between emission intensity and temperature.

integrated with a commercial UV LED chip, which converts UV light to pure and strong blue-emitting light. In addition, this N-CDs/LDH composite material shows high UV-resistance and storage stability, which would guarantee its prospective applications in optical and optoelectronic devices.

Acknowledgements

Notes and references

1 (a) S. N. Baker and G. A. Baker, *Angew. Chem., Int. Ed.*, 2010, **49**, 6726; (b) S. Qu, X. Wang, Q. Lu, X. Liu and L. Wang, *Angew. Chem., Int. Ed.*, 2012, **51**, 12215; (c) H. Li, Z. Kang, Y. Liu and S. T. Lee, *J. Mater. Chem.*, 2012, **22**, 24230; (d) S. C. Ray, A. Saha, N. R. Jana and R. Sarkar, *J. Phys. Chem. C*, 2009, **113**, 18546.

2 (a) Y. P. Sun, B. Zhou, Y. Lin, W. Wang, K. A. Fernando, P. Pathak, M. J. Meziani, B. A. Harruff, X. Wang, H. Wang, P. G. Luo, H. Yang, M. E. Kose, B. Chen, L. M. Veca and S. Y. Xie, *J. Am. Chem. Soc.*, 2006, **128**, 7756; (b) S. Zhu, Y. Song, X. Zhao, J. Shao, J. Zhang and B. Yang, *Nano Res.*, 2015, **8**, 355; (c) Q. Xu, Y. Liu, C. Gao, J. Wei, H. Zhou, Y. Chen, C. Dong, T. S. Sreeprasad, N. Li and Z. Xia, *J. Mater. Chem. C*, 2015, **3**, 9885.

3 (a) S. Zhu, Q. Meng, L. Wang, J. Zhang, Y. Song, H. Jin, K. Zhang, H. Sun, H. Wang and B. Yang, *Angew. Chem., Int. Ed.*, 2013, **52**, 3953; (b) Z. Qian, J. Ma, X. Shan, H. Feng and L. Shao, *Chem. – Eur. J.*, 2014, **20**, 2254.

4 (a) Y. Mu, N. Wang, Z. Sun, J. Wang, J. Li and J. Yu, *Chem. Sci.*, 2016, **7**, 3564; (b) H. Ding, S. B. Yu, J. S. Wei and H. M. Xiong, *ACS Nano*, 2016, **10**, 484; (c) L. Guo, J. Ge, W. Liu, G. Niu, Q. Jia, H. Wang and P. Wang, *Nanoscale*, 2016, **8**, 729; (d) S. Sarkar, M. Sudolská, M. Dubecký, C. J. Reckmeier, A. L. Rogach, R. Zbořil and M. Otyepka, *J. Phys. Chem. C*, 2016, **120**, 1303.

5 (a) P. Ayala, R. Arenal, M. Rümmeli, A. Rubio and T. Pichler, *Carbon*, 2010, **48**, 575; (b) K. Gong, F. Du, Z. Xia, M. Durstock and L. Dai, *Science*, 2009, **323**, 760.

6 (a) Q. Li, S. Zhang, L. Dai and L. S. Li, *J. Am. Chem. Soc.*, 2012, **134**, 18932; (b) Y. Li, Y. Zhao, H. Cheng, Y. Hu, G. Shi, L. Dai and L. Qu, *J. Am. Chem. Soc.*, 2012, **134**, 15; (c) Z. Li, H. Yu, T. Bian, Y. Zhao, C. Zhou, L. Shang, Y. Liu, L. Z. Wu, C. H. Tung and T. Zhang, *J. Mater. Chem. C*, 2015, **3**, 1922.

7 (a) D. Qu, Z. Sun, M. Zheng, J. Li, Y. Zhang, G. Zhang, H. Zhao, X. Liu and Z. Xie, *Adv. Opt. Mater.*, 2015, **3**, 360;

(b) A. Cayuela, S. R. Kennedy, M. L. Soriano, C. D. Jones, M. Valcárcel and J. W. Steed, *Chem. Sci.*, 2015, **6**, 6139; (c) Z. Wang, B. Fu, S. Zou, B. Duan, C. Chang, B. Yang, X. Zhou and L. Zhang, *Nano Res.*, 2016, **9**, 214; (d) Q. Li, M. Zhou, Q. Yang, Q. Wu, J. Shi, A. Gong and M. Yang, *Chem. Mater.*, 2016, **28**, 8221.

8 (a) Q. Wang and D. O'Hare, *Chem. Rev.*, 2012, **112**, 4124; (b) M. Q. Zhao, Q. Zhang, J. Q. Huang and F. Wei, *Adv. Funct. Mater.*, 2012, **22**, 675; (c) R. Tian, D. Yan and M. Wei, *Struct. Bonding*, 2015, **166**, 1.

9 (a) A. M. Fogg, V. M. Green, H. G. Harvey and D. O'Hare, *Adv. Mater.*, 1999, **11**, 1466; (b) Z. P. Xu, G. S. Stevenson, C. Q. Lu, G. Q. Lu, P. F. Bartlett and P. P. Gray, *J. Am. Chem. Soc.*, 2006, **128**, 36; (c) M. Q. Zhao, Q. Zhang, X. L. Jia, J. Q. Huang, Y. H. Zhang and F. Wei, *Adv. Funct. Mater.*, 2010, **20**, 677.

10 (a) J. Sun, H. Liu, X. Chen, D. G. Evans, W. Yang and X. Duan, *Adv. Mater.*, 2013, **25**, 1125; (b) L. Wang, Y. Zhu, J. Q. Wang, F. Liu, J. Huang, X. Meng, J. M. Basset, Y. Han and F. S. Xiao, *Nat. Commun.*, 2015, **6**, 6957.

11 (a) D. Yan, J. Lu, J. Ma, S. Qin, M. Wei, D. G. Evans and X. Duan, *Angew. Chem., Int. Ed.*, 2011, **50**, 7037; (b) S. Li, J. Lu, M. Wei, D. G. Evans and X. Duan, *Adv. Funct. Mater.*, 2010, **20**, 2848.

12 (a) F. Wang, Z. Xie, H. Zhang, C. Y. Liu and Y. G. Zhang, *Adv. Funct. Mater.*, 2011, **21**, 1027; (b) D. Pan, J. Zhang, Z. Li, Z. Zhang, L. Guo and M. Wu, *J. Mater. Chem.*, 2011, **21**, 3565; (c) Z. Xie, F. Wang and C. Y. Liu, *Adv. Mater.*, 2012, **24**, 1716.

13 (a) M. Xu, G. He, Z. Li, F. He, F. Gao, Y. Su, L. Zhang, Z. Yang and Y. Zhang, *Nanoscale*, 2014, **6**, 10307; (b) Y. Hao, Z. Gan, J. Xu, X. Wu and P. K. Chu, *Appl. Surf. Sci.*, 2014, **311**, 490; (c) M. Sun, S. Qu, Z. Hao, W. Ji, P. Jing, H. Zhang, L. Zhang, J. Zhao and D. Shen, *Nanoscale*, 2014, **6**, 13076; (d) F. Wang, Z. Xie, B. Zhang, Y. Liu, W. Yang and C. Y. Liu, *Nanoscale*, 2014, **6**, 3818.

14 (a) C. C. Shih, P. C. Chen, G. L. Lin, C. W. Wang and H. T. Chang, *ACS Nano*, 2015, **9**, 312; (b) D. Mosconi, D. Mazzier, S. Silvestrini, A. Privitera, C. Marega, L. Franco and A. Moretto, *ACS Nano*, 2015, **9**, 4156; (c) C. Shen, J. Wang, Y. Cao and Y. Lu, *J. Mater. Chem. C*, 2015, **3**, 6668; (d) Y. Wang, S. Kalytchuk, L. Wang, O. Zhovtiuk, K. Cepe, R. Zboril and A. L. Rogach, *Chem. Commun.*, 2015, **51**, 2950; (e) Y. Chen, M. Zheng, Y. Xiao, H. Dong, H. Zhang, J. Zhuang, H. Hu, B. Lei and Y. Liu, *Adv. Mater.*, 2016, **28**, 312.

15 Y. Song, S. Zhu, S. Zhang, Y. Fu, L. Wang, X. Zhao and B. Yang, *J. Mater. Chem. C*, 2015, **3**, 5976.

16 M. Jobbágy and N. Iyi, *J. Phys. Chem. C*, 2010, **114**, 18153.

17 P. Yu, X. Wen and Y. R. Toh, *J. Phys. Chem. C*, 2012, **116**, 25552.

This journal is © The Royal Society of Chemistry 2017

J. Mater. Chem. C, 2017, **5**, 3536–3541 | **3541**